ADVANCED MATERIALS

Supporting Information

for *Adv. Mater.,* DOI: 10.1002/adma.202104769

Stretchable Thin Film Mechanical-Strain-Gated Switches and Logic Gate Functions Based on a Soft Tunneling Barrier

Soosang Chae, Won Jin Choi, Ivan Fotev, Eva Bittrich, Petra Uhlmann, Mathias Schubert, Denys Makarov, Jens Wagner, Alexej Pashkin, and Andreas Fery**

Supporting Information

Stretchable Thin-Film Mechanical-Strain-Gated Switches and Logic Gate Functions Based on a Soft Tunneling Barrier

Soosang Chae[*], Won Jin Choi[†], Ivan Fotev[†], Eva Bittrich, Petra Uhlmann, Mathias Schubert, Denys Makarov, Jens Wagner, Alexej Pashkin, Andreas Fery[*]

This supporting information includes:

Other supplementary materials for this manuscript include the following:
Movie S1

S1. Fabrication of strain-gated stretchable electric switch

The intermediate layer is the key part determining the strain gated switch behavior of the structure. We also used polydimethylsiloxane (PDMS) because of its intrinsic softness, Poisson's ratio, and appropriate insulating behavior.

We investigated various strategies to fabricate the thin PDMS intermediate layer: (1) vapor-phase PDMS deposition [R1], (2) inkless μcontact printing of a PDMS stamp [R2], and (3) general spin-coating with a diluted PDMS solution. However, because of the poor reproducibility and complexity of these conventional methods, we developed and optimized a new fabrication method: self-diffusion of a low molecular weight (low-MW) PDMS (Sylgard 184, Dow corning) layer from a thick PDMS substrate. Inspired by the well-known hydrophobic recovery phenomenon of surface-oxidized PDMS [R3], we designed an intermediate thin PDMS layer with reliable reproducibility and precise controllability to fit our device. When optimizing the fabrication, we found that the diffusion process of the low-MW PDMS accelerated dramatically under high-vacuum conditions compared with the diffusion process under atmospheric conditions. The pressure dependence of the diffusion coefficient of the PDMS molecules [R4] might explain this acceleration. This finding enabled us not only to reduce the fabrication time but also increase the reproducibility of the process because the whole device fabrication procedure, including two depositions of metal thin films, can be carried out in a high-vacuum chamber. The vacuum pressure, aging time, and crack density of the metal film as a diffusion path are key aspects affecting the performance of the intermediate layer. For our practical approach, we optimized the vacuum conditions (8 h at 6.0×10^{-6} mbar) and only varied the crack density of the first metal thin film to observe the effect of the PDMS layer thickness on the switching performance. As a result, we found that a higher crack density of the deposited metal thin film led to a higher threshold strain corresponding to the insulator-to-metal transition in the device, as shown in Fig. 2f.

Interestingly, the diffusion of low-molecular-weight (low-Mw) PDMS from the PDMS substrate through the first deposited metal layer led to the spontaneous formation of a thin PDMS layer on the surface of the first metal layer. Of course, although the inter-gap between each gold flakes of first layer is impregnated with the diffused PDMS, they did not hinder the inter-conduction path across the thinned barrier layer when it is stretched. Hence, the PDMS substrate used in the present study not only serves as a substrate but also contributes to the formation of the intermediate tunneling barrier layer as a reservoir. The diffusion process generally takes a few weeks when the sample is kept at atmospheric pressure. To accelerate this process, we induced cracking of the first metal thin film and incubated the sample under high

vacuum, which dramatically decreased the diffusion time of the PDMS. Atomic force microscopy (AFM) characterization (Supplementary Figure S1) of the sample before and after cracking (i, ii), and vacuum incubation (iii, iv) showed the formation of cracks in the metal film; these cracks provided channels for the molecular diffusion while ensuring complete formation of a low-Mw PDMS layer at the surface of the first metal layer. Note that the vacuum incubation time and the amount of pre-stretching (%) can vary the thickness of intermediate layer. After the formation of the ultra-thin PDMS film, we deposited the second metal thin film in the same manner as the first metal layer (iv). Finally, a high-angle annular dark-field scanning transmission electron microscopy (HAADF-STEM) image of the interface (white dashed-line box in Fig. 2a) and the energy-dispersive X-ray spectroscopy (EDS) line-profile of Si (*i.e.*, the distinguishable atoms of PDMS) confirmed that the thin PDMS intermediate layer existed between the bilayer metal thin film (Fig. 2a). This approach enables us to readily create an ultrathin soft barrier layer without any chemical modifications or surface treatment, which could lead to unwanted electrical impurities that hinder the unambiguous electrical characterization of the system.

S2. Calculation of tunneling induced strain dependence conductance

We have conducted Terahertz time-domain spectroscopy (THz-TDS) measurements on a stretched polydimethylsiloxane (PDMS) sample to evaluate the thinning. In particular, this experimental method measures precisely the "time of flight" of a short electromagnetic pulse through a sample [R5]. This quantity is directly proportional to the thickness of a sample. Thus, THz-TDS allows us to determine the variation of the PDMS thickness as a function of strain. Certainly, the THz-TDS is dominated by the time delay in the thick PDMS substrate – the thickness of the gold layers and the PDMS barrier layer between them is negligible compared to the substrate. However, it is reasonable to assume that both PDMS layers (the substrate and the thin barrier layer) deform in the same way when the strain is applied. Therefore, the relative change of the PDMS substrate thickness measured by the THz-TDS should reflects the actual thinning of the tunneling barrier enabling us to model the tunneling current in the investigated structure. The normalized thickness change of whole PDMS sample with deposited bi-layer metal electrode derived by the plot of (n-1)l with various applied strain, n is refractive index of

intermediate PDMS layer at THz range and l is a thickness (Supplementary Figure S2). Note that the change of refractive index in the stretched PDMS is negligible compared to its thickness variation. This fact follows from the reported THz elasto-optical constant of PDMS of -1.75×10^{-10} m^2/N and its Young's modulus of 10^6 Pa [R6]. The estimated change of the refractive index $\Delta n \approx -8.8\times10^{-5}$ for a strain $\varepsilon = 1.0$. Obviously, $\Delta n \ll \Delta l$ since the measured quantity $(n-1)l$ varies by tens of percent due to the thickness decrease.

Hence, the normalized value shown in Fig. 2(c) depicts the PDMS thickness as a function of strain. It has been measured at two positions: in the center of the PDMS substrate and half way off-center. Both measurements demonstrate almost the same variation indicating that the sample is homogeneously deformed. The normalized average value shown in Supplementary Figure S2 shows the PDMS thickness as a function of strain. It was measured at two positions: in the center of the PDMS substrate and halfway off-center. Note that the uniform thickness thinning through the sample is well consistent to the conductivity transition over large area (5 cm × 5 cm) as shown in Supplementary Figure S17.

Knowing the thickness variation of the PDMS layer under strain, we can model the conductance of the structure using the tunneling model proposed by Simmons.[26] In the limit of low voltages V, when the potential drop across the barrier is much smaller than the average barrier height ($eV << \varphi$), the tunneling current should be directly proportional to V. This condition indeed holds for the studied PDMS sample, as evidenced by the current–voltage (I–V) curves recorded for different strains. All of the I–V curves are approximately linear (R^2 in inset) over the whole applied strain range ($\varepsilon = 0 \rightarrow 1$) (Supplementary Figure S4). Note the different current scales for different applied strains. Therefore, the generalized equation for the tunneling current can be simplified to[27]

$$j = \frac{\sqrt{2m\varphi}}{s(\varepsilon)}\left(\frac{e}{h}\right)^2 V\, exp\left[-\frac{4\pi s(\varepsilon)}{h}\sqrt{2m\varphi}\right], \qquad (1)$$

where $s(\varepsilon)$ is the barrier thickness dependent on strain ε and m is the electron mass. We assume that, for moderate strains ($\varepsilon < 0.5$), the thin PDMS layer is bonded to the substrate and that its change in relative thickness follows the substrate deformation characterized by the TDS-THz measurements. The initial thickness (without strain) was set to 12 nm, which is comparable to the value reported in literature[R8-R10]; this value was measured by ellipsometry on a model sample on a Si-wafer substrate (see details in Supplementary Information S4 and Supplementary Figure S5). The calculated conductance of the switch device is shown in Fig. 2c together with the measured values. The barrier height was set to φ= 2.3 eV to achieve the best agreement with the experimental data. Obviously, for $\varepsilon > 0.5$, the conductance saturates and does not demonstrate the model's prediction of exponential growth with increasing strain. We speculate that, at such large strain, the thin PDMS barrier layer begins to slip and loses its bonding with the substrate. As a result, the barrier thickness does not vary as the applied strain is increased further, leading to the observed current saturation. Presumably, the lateral conductivity (*via* intraconduction) also must change at such large strain regions. For other future material configurations, as evident from Supplementary Figure S6, both the initial thickness of the barrier layer (s_0) and the barrier height (φ) between the metal/barrier interface jointly determine the switching ratio: larger on-to-off ratio values are expected for thicker and higher barriers. However, an excessively thick barrier in either height or initial thickness could give rise to a huge resistivity, which implies a certain limitation to the expected transition value for this design.

S3. Theoretical thickness thinning of soft barrier layer by FEM

Finite-element software (COMSOL 5.5) was used to calculate the theoretical thickness change of the Au/nano PDMS/Au/Bulk PDMS structures, which provided insight into the hyperelastic deformation behavior. The width (and length) of the rectangular structure was 100 nm. Because the model system was thin (30 nm of Au and 12 nm of nano-PDMS), a minimum element size of 2.2 nm was used. As a substrate, 50 nm-thick bulk PDMS was adopted. We

enforced a boundary condition on either end of the Au/nano PDMS/Au/bulk PDMS structure: at one end we sweep described displacements in the *y*-axis direction; at the opposite end, we place fixed boundary conditions such that no displacement is allowed at the end. Two elastic models were tested for PDMS formation under elongation: the St. Venant Kirchhoff model and the linear elastic model. The St. Venant Kirchhoff model was found to well fit the experimental results as shown in Fig.S8. Lame parameter λ and μ for PDMS were 6.93 GPa and 0.77 GPa, respectively. [R7]

S4. Measurement of initial thickness of the intermediate barrier layer

We determined the initial thickness of the intermediate PDMS tunneling barrier by spectroscopic ellipsometry. Compared with the thickness evaluated from the cross-sectional HRTEM image (Fig. 2a), the thickness of the nanometric thin film is modeled as an average value over an area of square centimeters from ellipsometric data, resembling the area used for conductance measurements. However, ellipsometric analysis of the real strain gated switch stretchable device was not successful because of the intrinsic softness and low reflectivity of the PDMS substrate and the change in optical constants of the first layer of the metal thin film as a consequence of the diffusion of the low-Mw PDMS. To solve this technical problem, we fabricated model samples on rigid Si/SiO_2 wafer substrates and formed the thin PDMS layer via the contact printing method. The method is described as follows: First, a cured PDMS slab similar to that used for the strain gated switch sample was prepared. Second, the PDMS slab was contacted with the SiO_2/Si wafer and heated at 80 °C for 2 h. The free PDMS oligomer on the surface of the PDMS slab was transferred to the SiO_2/Si surface by the driving force of a concentration gradient. Repeating this contact printing (CP in the horizontal axis of Supplementary Figure S5) increased the thickness of the thin PDMS layer, as shown in Supplementary Figure S5. The thickness was saturated at 12 nm beyond six contact printing cycles because of the equilibrium in the concentration gradient at the interface, which means that the SiO_2/Si surface on the wafer substrate was fully covered by the printed PDMS oligomer.

Regarding the real sample of the strain gated switch stretchable substrate, the free PDMS oligomer, which remained inside the bulk PDMS substrate underneath the first metal layer, diffused out and formed the thin intermediate barrier layer. (A description of the fabrication procedure in section Supplementary Information S1). The driving force of this spontaneous phenomenon is the reduction of the surface are of the Au thin film because the surface energy of the free oligomer is lower than that of the Au. This reaction continued until the surface was fully covered by free PDMS oligomer, similar to that obtained for the aforementioned model

sample. The independency of the saturation point on the type of substrate material was demonstrated by water-contact-angle measurements of contact-printed thin PDMS layers on various types of substrates (Supplementary Figure S16). Irrespective of the materials, the water contact angles were 103° for 24 h of contact-printing time. On the basis of these results, we assumed that the initial thickness of the intermediate PDMS barrier in the strain gated switch device had the same thickness as the thin PDMS layer formed by contact-printing on the model sample.

S5. Modulation of initial thickness of the soft barrier layer

The experimental conditions of the diffusion process for the soft PDMS barrier layer can modulate the tendency of the strain gated switch transition of the structure. Maintaining the applied strain during the diffusion process gave rise to an increase in the number of voids in the first metal layer because of the separation of metal domains, which accelerates the diffusion of low-Mw PDMS and leads to the formation of the soft barrier layer with higher thickness. Fig. 2f shows the different strains applied during the diffusion process of the soft layer: 0%, 30%, and 80% of applied strain. Depending on the strain, the samples showed different strain gated switch transition tendencies.

Supplementary Reference

[R1] Jiao, K., Zhou, C., Becerra-Mora, N., Fiske, J., & Kohli, P. (2016). Vapor-enhanced covalently bound ultra-thin films on oxidized surfaces for enhanced resolution imaging. *Journal of Materials Chemistry C*, *4*(37), 8634-8647.

[R2] Kim, J. H., Hwang, H. S., Hahm, S. W., & Khang, D. Y. (2010). Hydrophobically recovered and contact printed siloxane oligomers for general-purpose surface patterning. *Langmuir*, *26*(15), 13015-13019.

[R3] Fritz, J. L., & Owen, M. J. (1995). Hydrophobic recovery of plasma-treated polydimethylsiloxane. *The Journal of adhesion*, *54*(1-4), 33-45.

[R4] Cussler, E. L., & Cussler, E. L. (2009). *Diffusion: mass transfer in fluid systems*. Cambridge university press.

[R5] Yun-Shik Lee, Principles of Terahertz Science and Technology, Springer, 2009

[R6] Madugani, R., Yang, Y., Ward, J. M., Riordan, J. D., Coppola, S., Vespini, V., ... & Chormaic, S. N. (2012). Terahertz tuning of whispering gallery modes in a PDMS stand-alone, stretchable microsphere. *Optics letters*, *37*(22), 4762-4764.

[R7] F.E. Hizir et al. Deformation of Stamp Features with Slanted Walls during Microcontact Printing, Proceedings of the 2014 COMSOL Conference in Boston https://www.comsol.jp/paper/download/194581/hizir_paper.pdf

[R8] Cowell III, E. W., Muir, S. W., Keszler, D. A., & Wager, J. F. (2013). Barrier height estimation of asymmetric metal-insulator-metal tunneling diodes. Journal of Applied Physics, 114(21), 213703.

[R9] El Kamel, F. (2015). Temperature dependent electron effective mass and barrier height in HfO2 based metal/oxide/metal devices. *Journal of Physics D: Applied Physics*, *48*(28), 285304.

[R10] Woo, M. H., Jang, B. C., Choi, J., Lee, K. J., Shin, G. H., Seong, H., ... & Choi, S. Y. (2017). Low-power nonvolatile charge storage memory based on MoS2 and an ultrathin polymer tunneling dielectric. *Advanced Functional Materials*, *27*(43), 1703545.

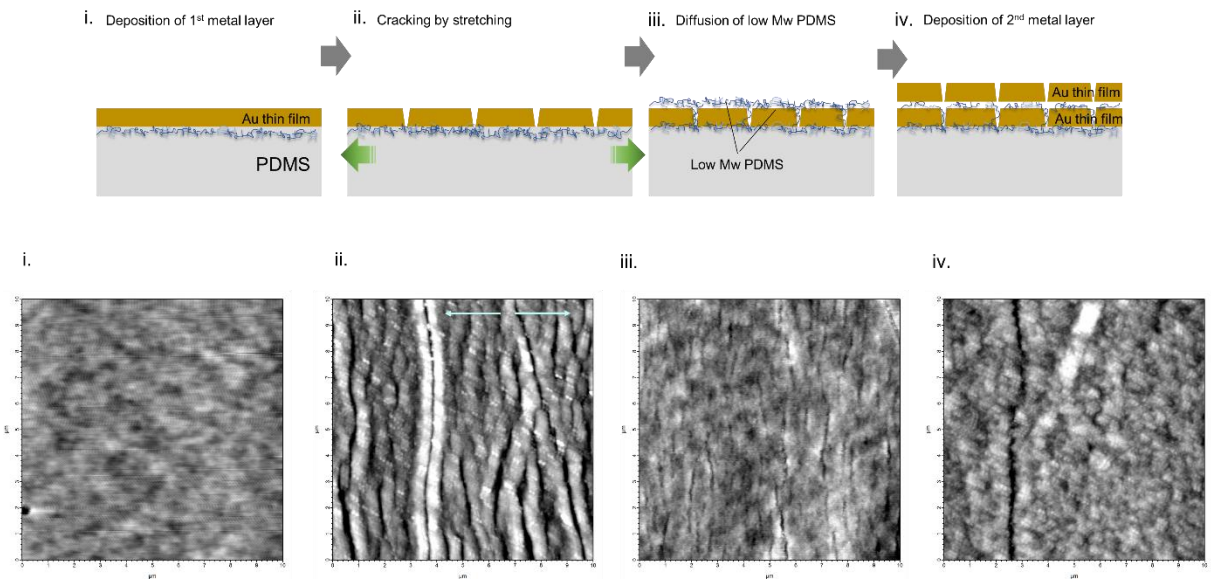

Figure S1. Schemes (i → iv) showing the fabrication of an strain gated switch stretchable device (top-row) and the corresponding AFM images of each process (bottom row). i) No significant features are observed on the surface of first metal layer as it is deposited. ii) Stretching the metal thin film induced lateral cracks perpendicular to the direction of stretching (blue arrows indicate the stretching direction). iii) Incubation of the sample under high vacuum resulted in flatness recovery via the diffusion of low-Mw PDMS and formation of a thin layer. iv) A second metal layer deposited onto the low-Mw PDMS layer covering the first metal layer. The surface thickness of the thin film increased from 17 nm to 29 nm to 49 nm during processes i–iv..

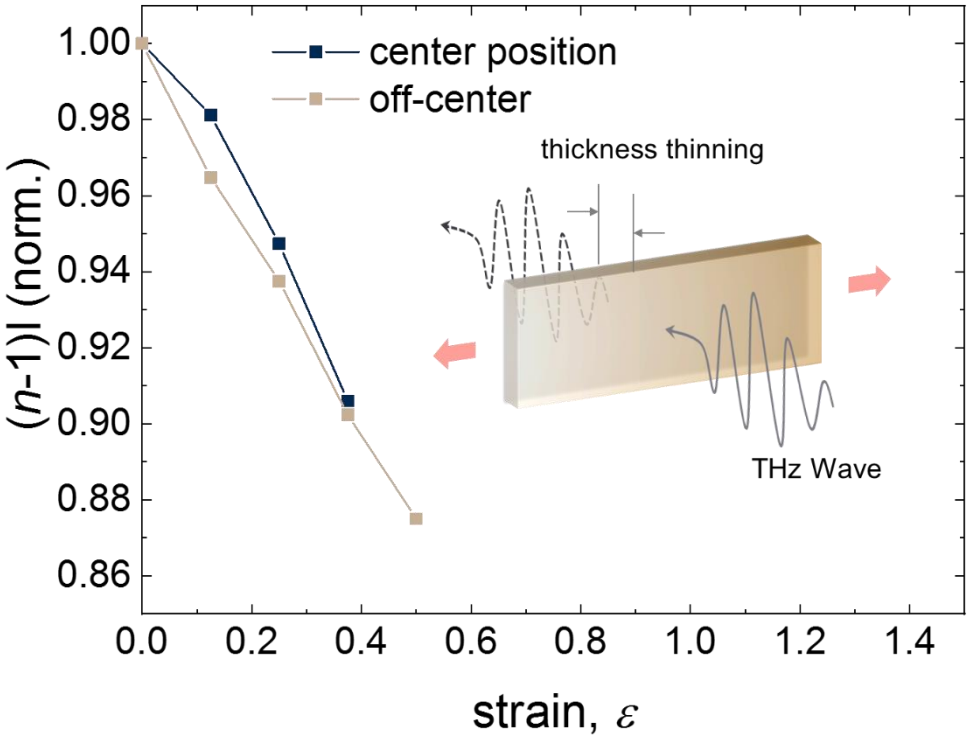

Figure S2. Experimental thickness thinning, as measured by THz-TDS spectroscopy.

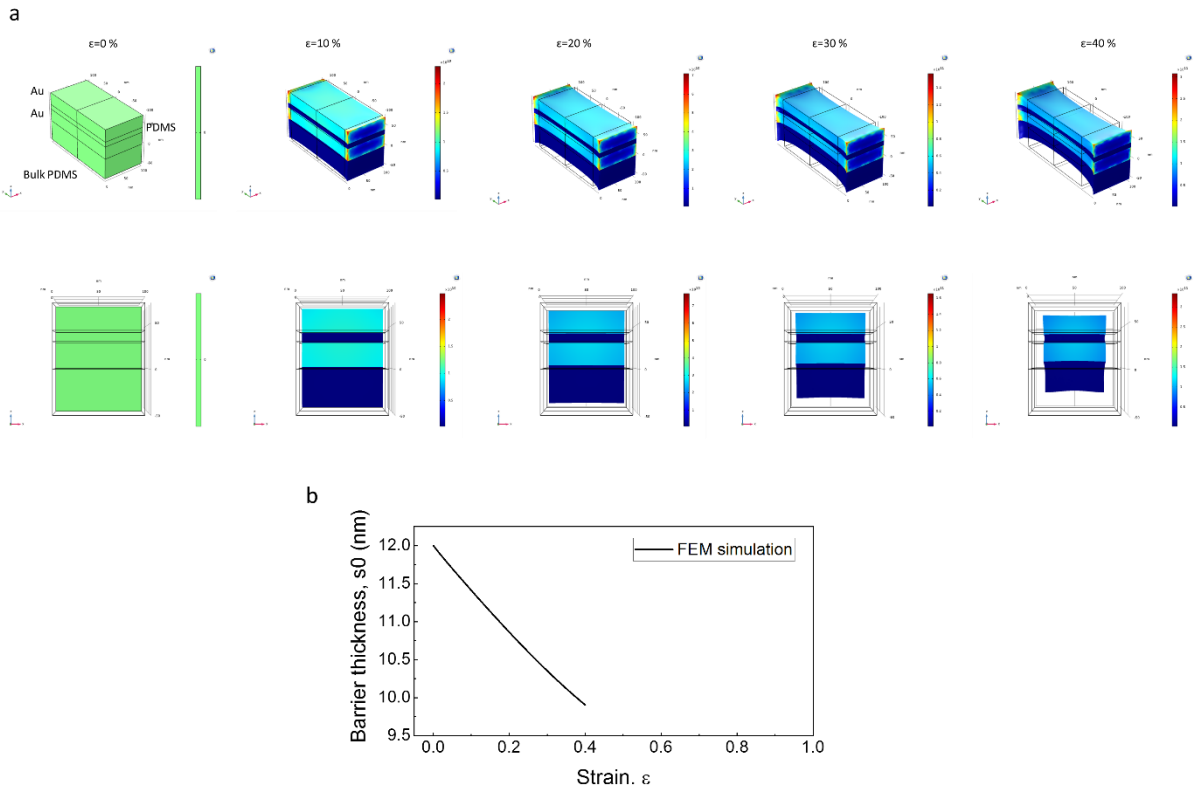

Figure S3. FEM simulation of Au/PDMS/Au structures. (a) Von Mises stress distribution as the uniaxial strain of the device increases according to the hyperelastic PDMS model (St. Venant Kirchhoff model). (b) The resultant thickness change of the PDMS soft barrier, as extracted from the FEM simulation.

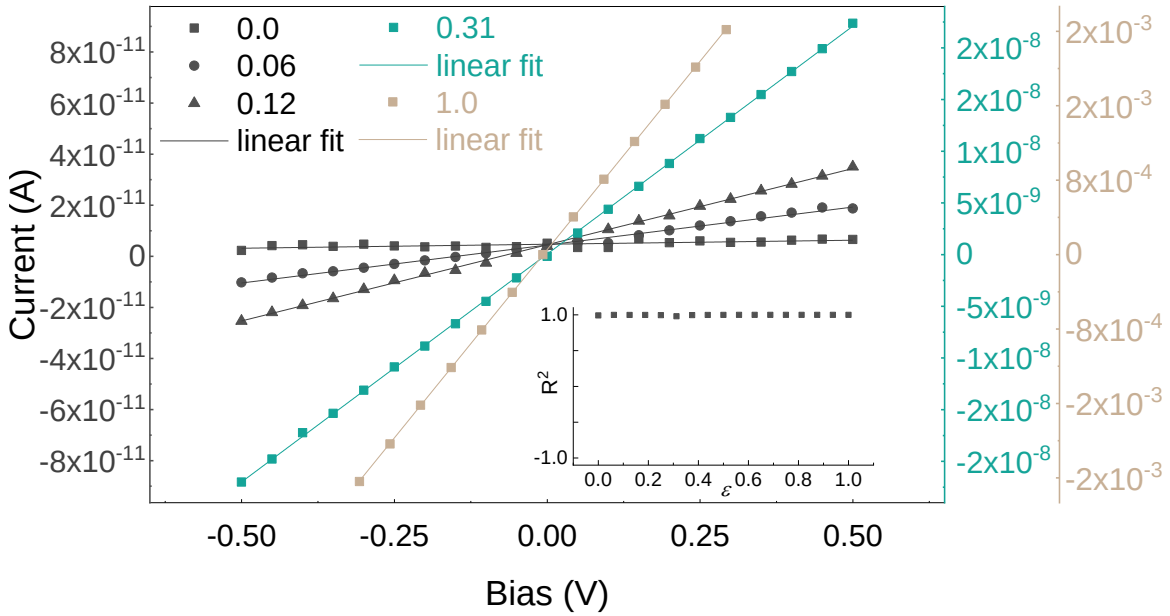

Figure S4. *I–V* curves of a Stretchable mechanical strain gated electric switch at different applied strains; all of the curves show linear behavior independent of the applied strain. Note that the current scales differ for different applied strains (inset: R^2 of the linear fit in the strain range from 0.0 to 1.0).

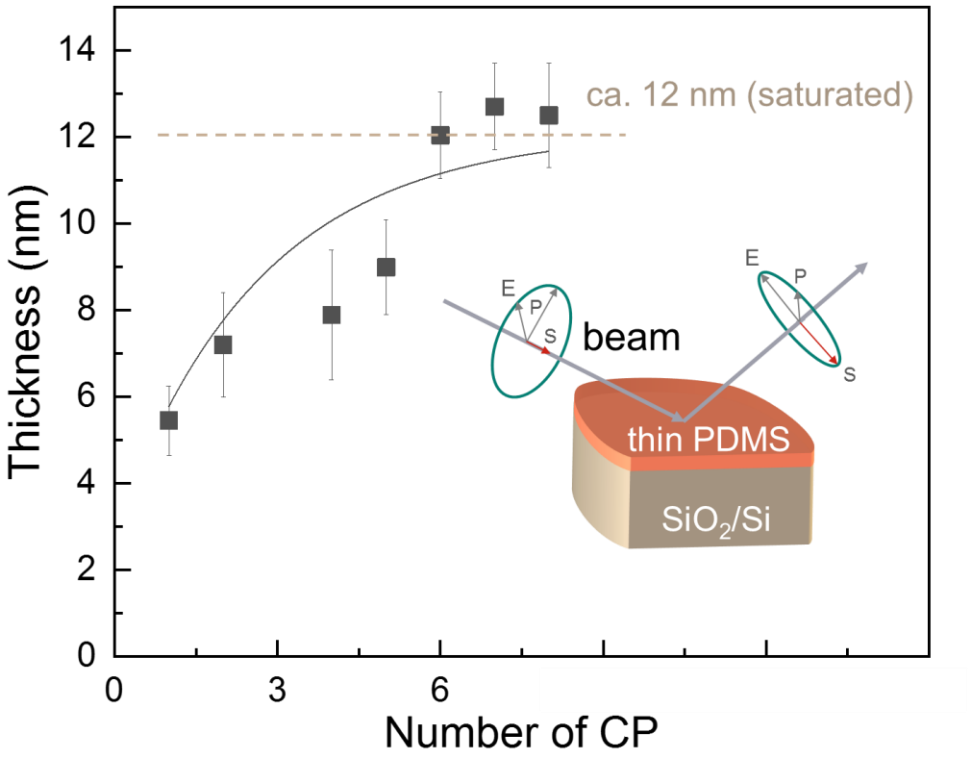

Figure S5. Determination of the initial barrier thickness ($s_{\varepsilon 0}$) measured by ellipsometry of the model sample (details are provided in Supplementary Information S4).

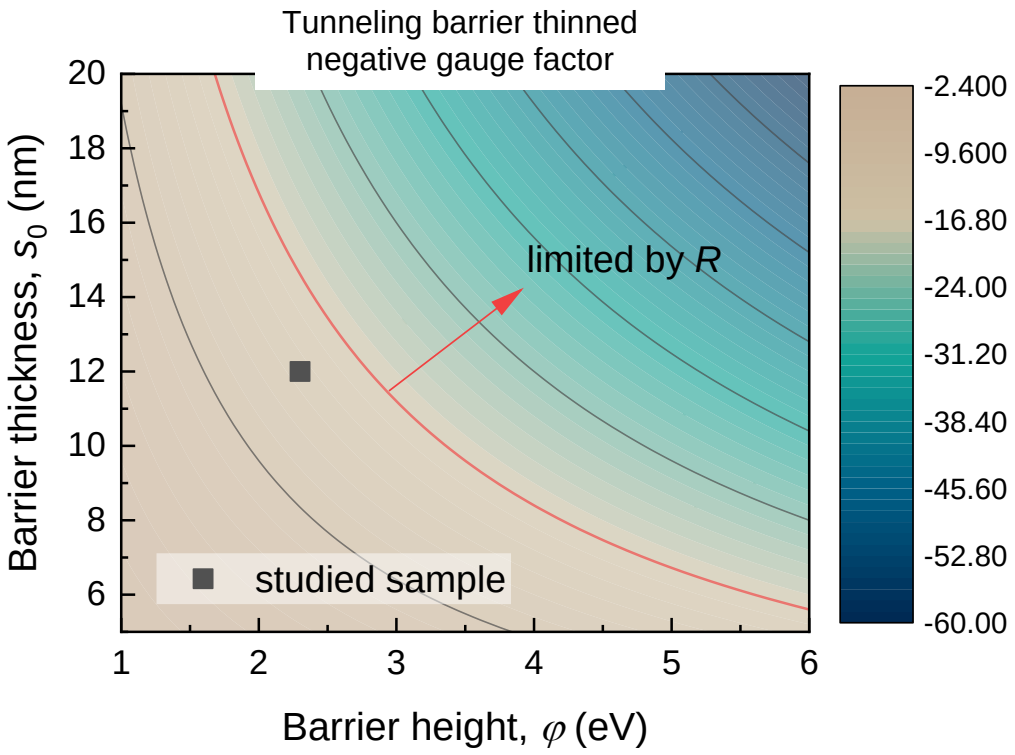

Figure S6. Expected strain gated switch as a function of the variation in the potential barrier height and the initial thickness of the soft barrier layer. Solid black squares (e.g., strain gated switch = −14.8) indicate the strain gated switch value for the sample studied in this work. Note that, beyond the red boundary line, the strain gated switch value could be limited in practical applications because of excessively high resistance. Each line corresponds to an strain gated switch level from −5 to −50 with a step of 10.

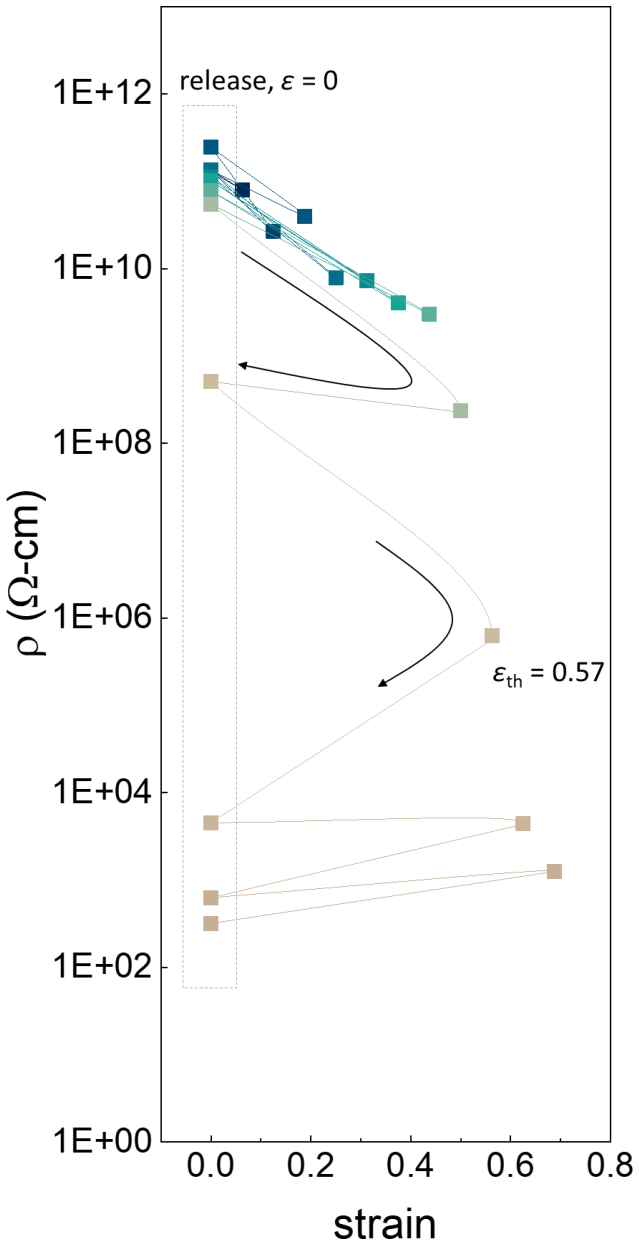

Figure S7. Irreversibility of the strain gated switch behavior beyond the threshold strain (ε = 0.57 for this sample). Presumably, when the strain is released to ε = 0, the whole structure is delaminated from the PDMS substrate because of the absence of any adhesive layer (e.g., a thin Ti or Cr layer), leading to structure deformation such as buckling or similar and showing the conversion to the low-resistivity state ($\rho < 10^4$ Ω·cm). Note that such reversibility is possible within a certain strain range because of the delamination of the whole layer from the substrate, which can be technically solved if adhesion at the interface between the first metal layer and the elastomer substrate is secure.

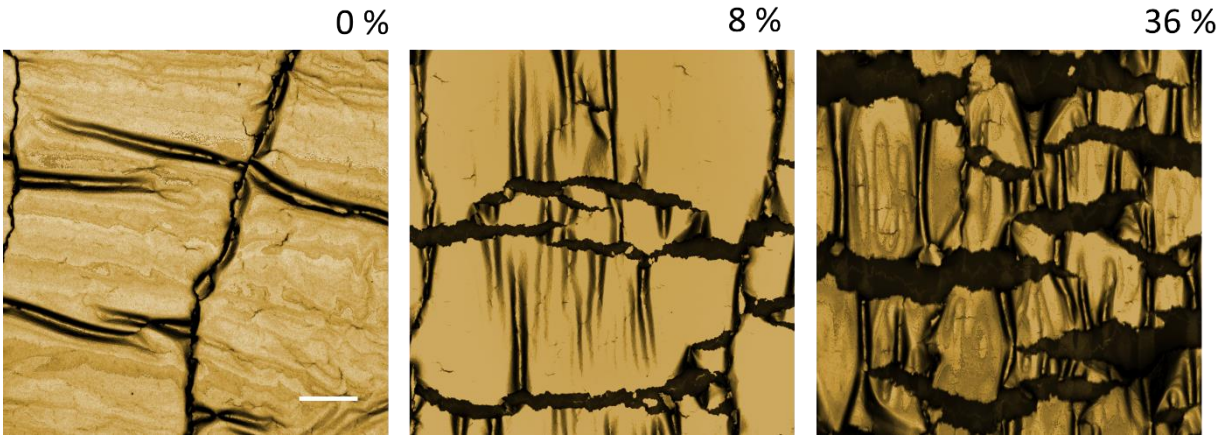

Figure S8. Optical microscopy image of a metal thin film (Au, 50 nm) deposited onto an elastomer substrate (PDMS) under various applied strains. Scale bar denotes 3 μm.

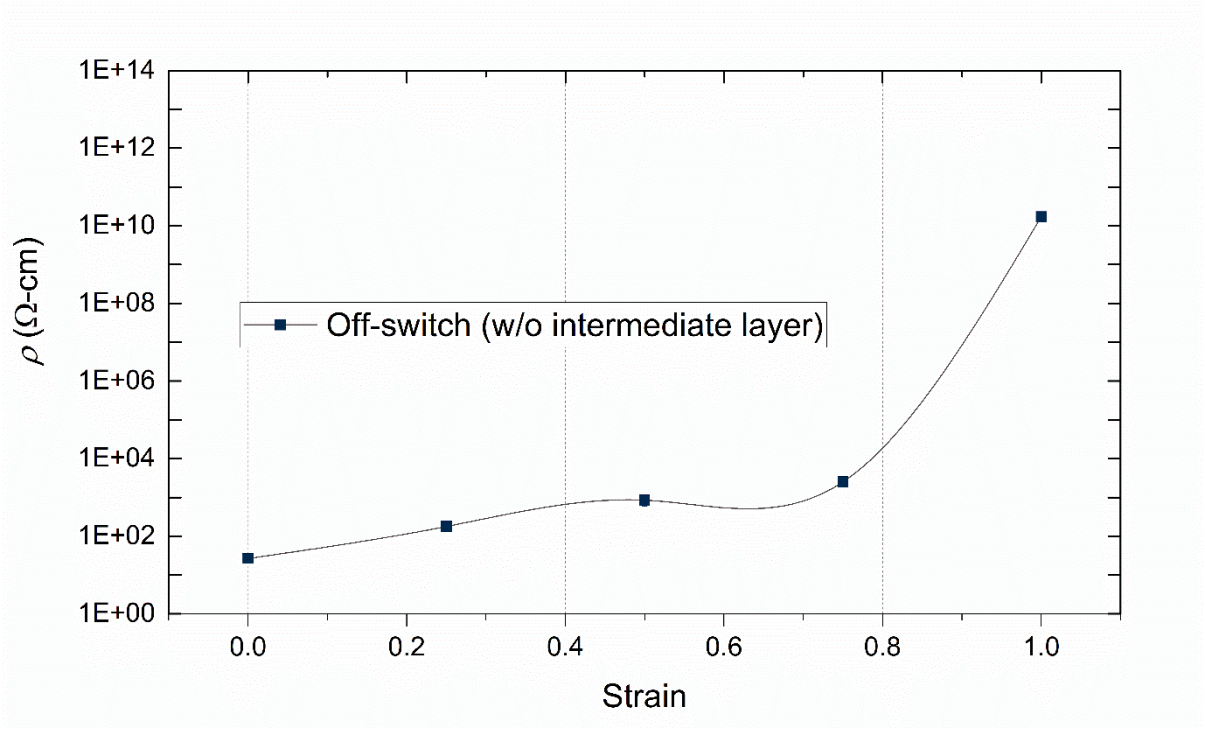

Figure S9. Off-switch feature of a bilayer sample with the same deposition thickness, but, in absence of intermediate layer.

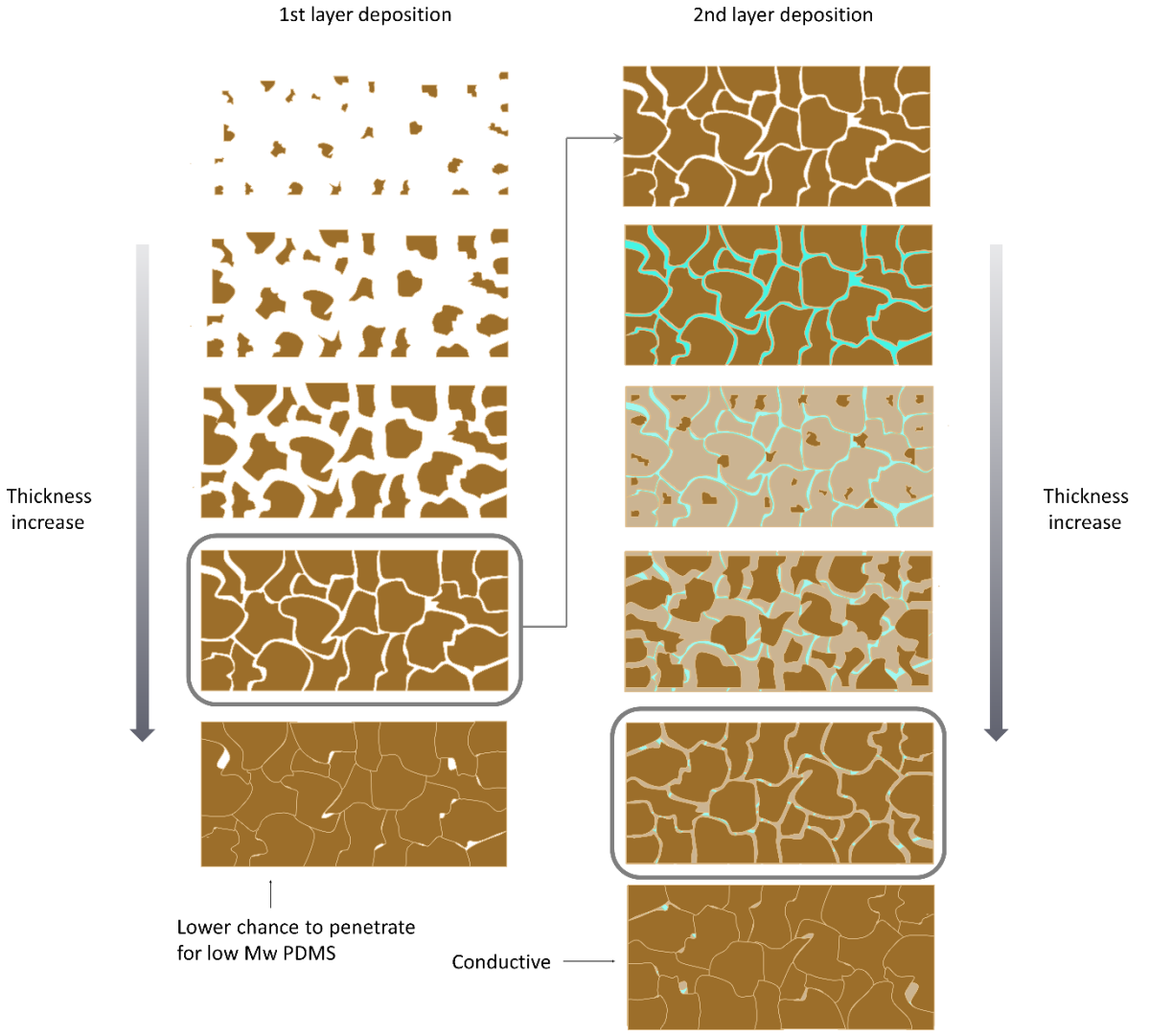

Figure S10. Optimization of the deposition thickness of the first (left column) and second (right column) layers. Both thicknesses are controlled to show either the mechanical strain induced electric switch or stretchable conductive interconnector behavior with respect to the percolation thresholds.

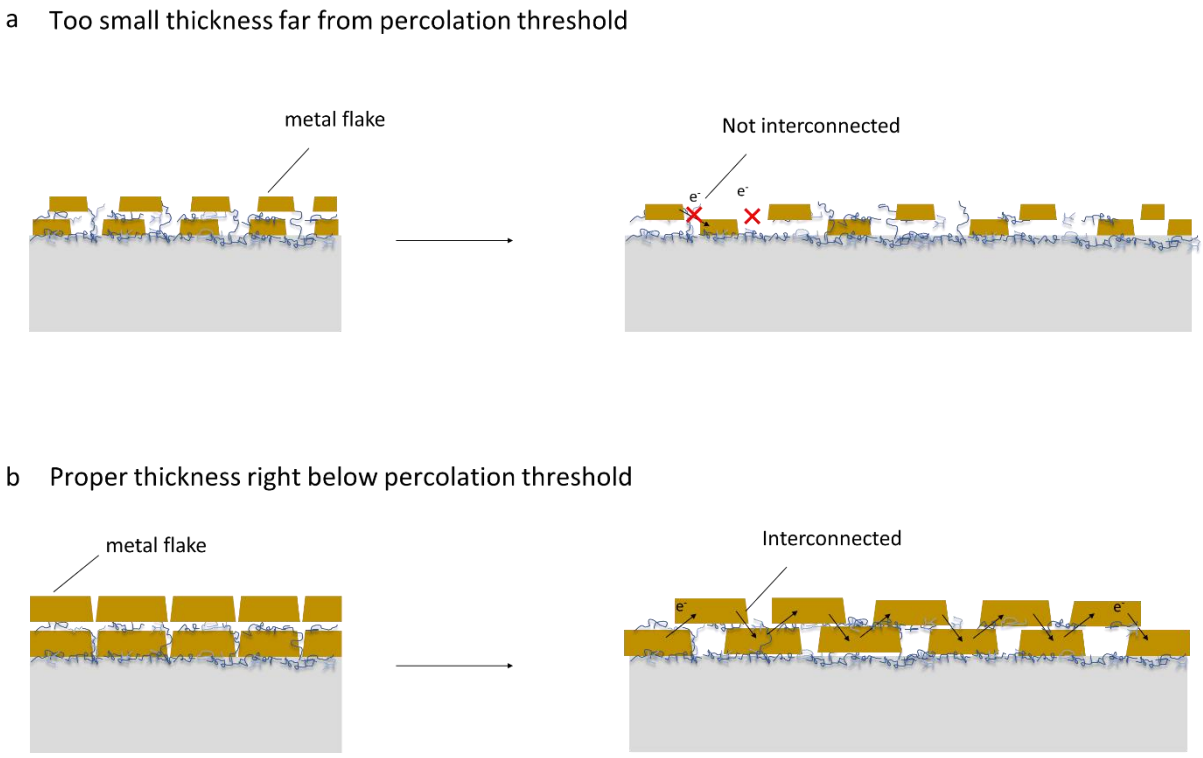

Figure S11. Optimization of the deposition thickness of each bilayer for percolation when it is stretched. **a**, constant insulator-like ("*A*" combination as shown in Fig. 3). b, on-switch behavior ("*C*" combination as shown in Fig. 3).

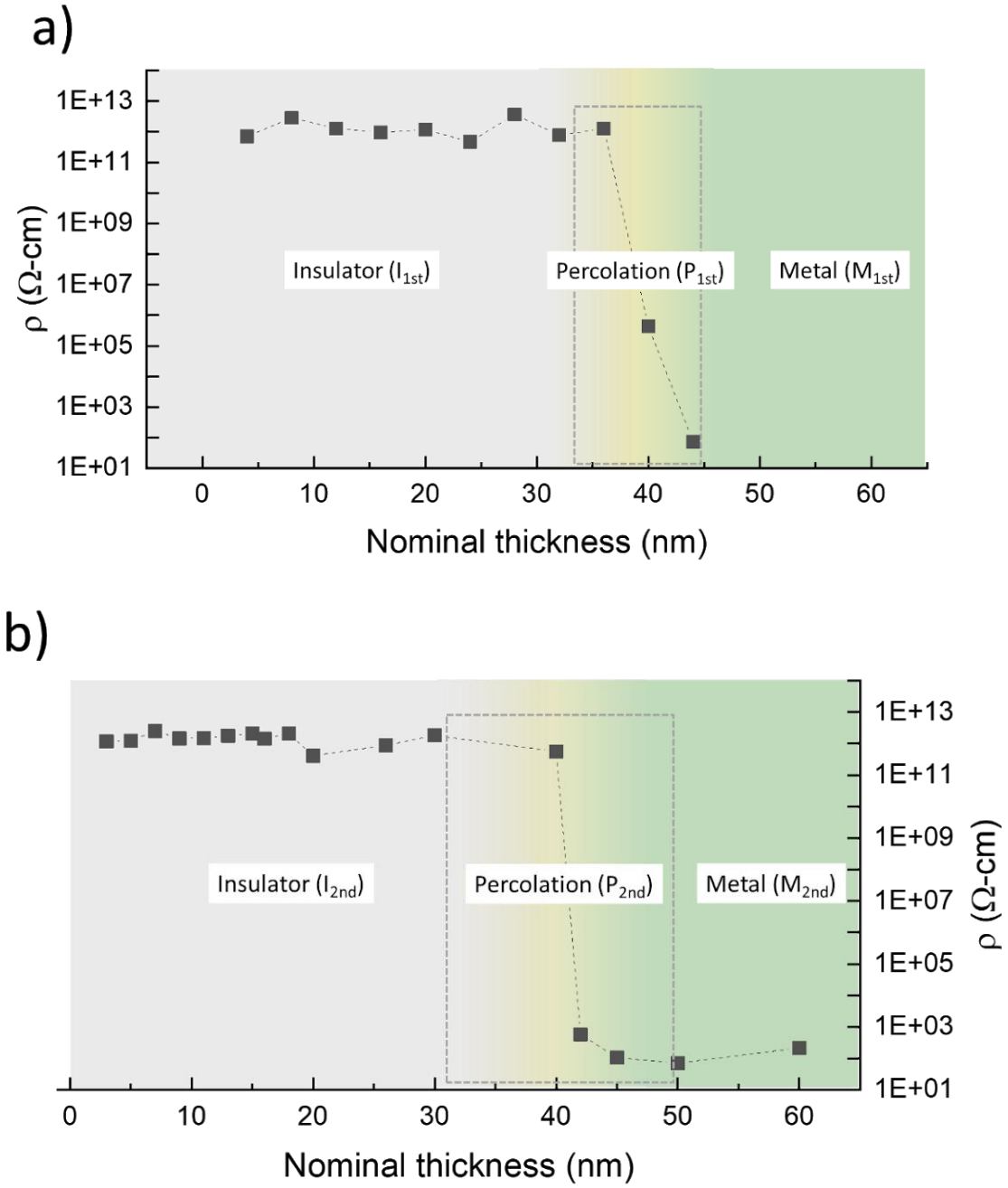

Figure S12. Determination of the percolation threshold thickness of the (a) first and (b) second metal layers.

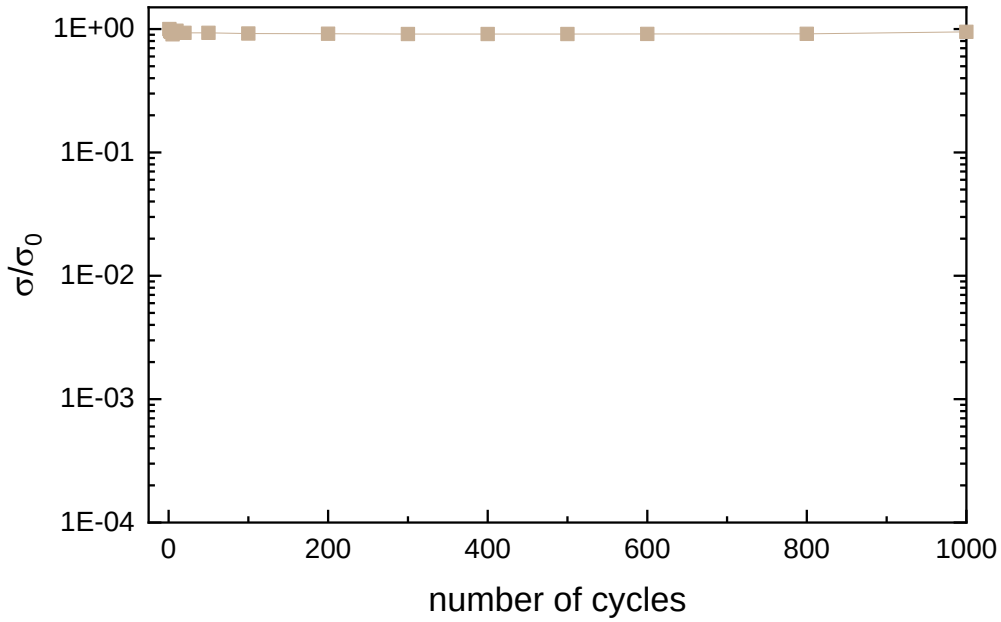

Figure S13. The strain-invariable electrode fabricated by the bimetal layer design is able to fully maintain its initial electrical conductivity for 1000 cycles.

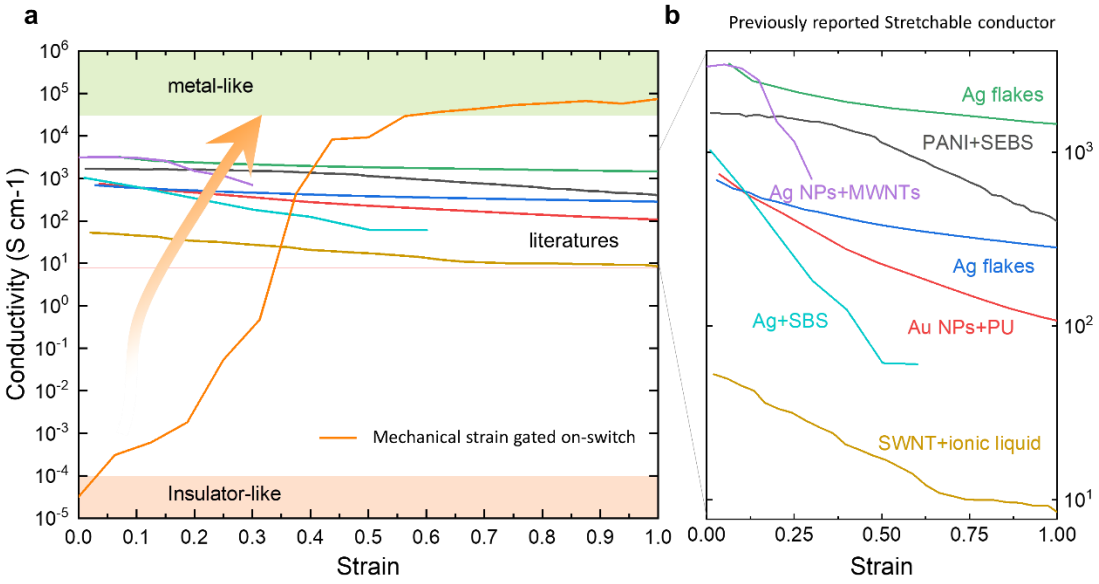

Figure S14. High performance of the stretchable mechanical strain gated electric switch. a, Measured DC conductivity with respect to applied strain of the stretchable electric switch, as compared with **b,** the corresponding DC conductivity for conventional stretchable electrodes previously reported in the literature.[17-23] The stretchable electric switch shows an extremely broad working range of conductivity. In particular, a very low initial conductivity (<10^{-4} S

cm^{-1}), such as in the case of an insulator, makes the development of stretchable mechanical strain gated electric switch.

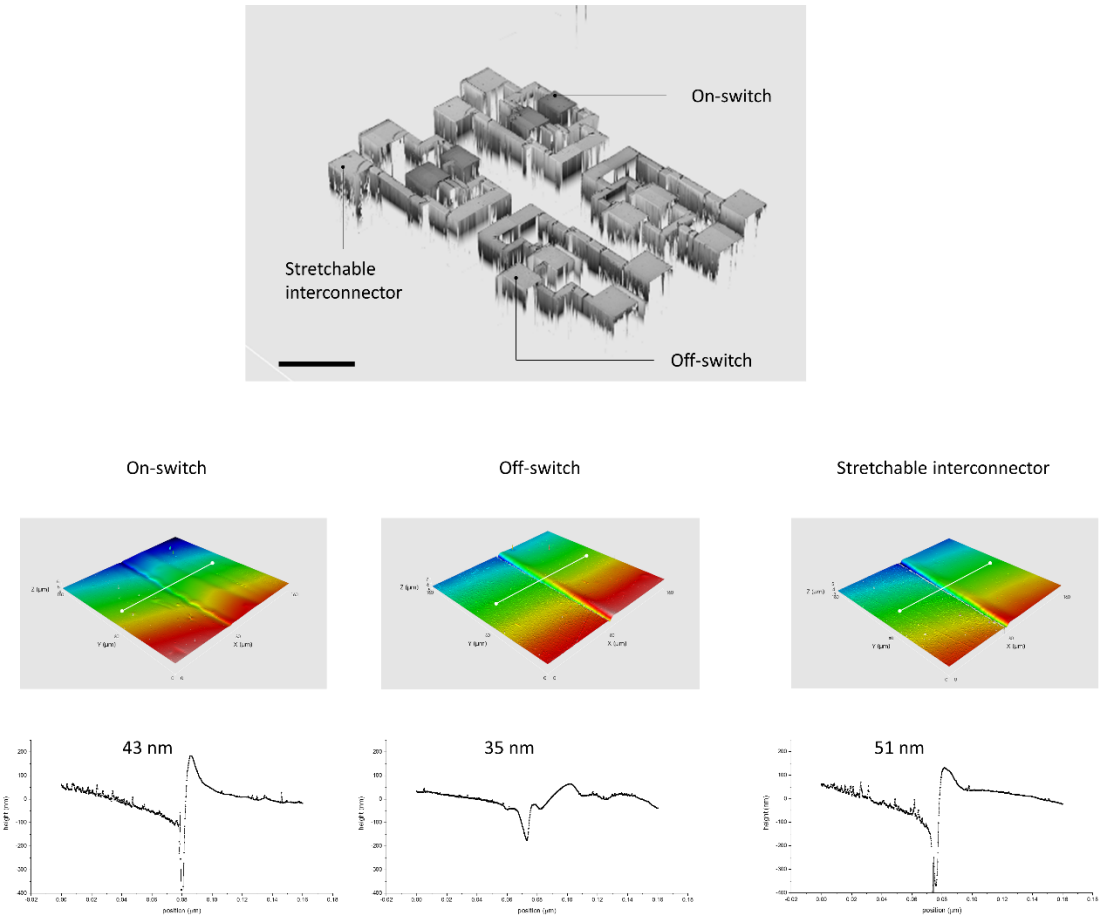

Figure S15. Thickness of each part in the stretchable thin film mechanical strain gated logic circuit. All the elements is comprised of metal thin film form within 50 nm thickness (scale bar denotes 100 μm).

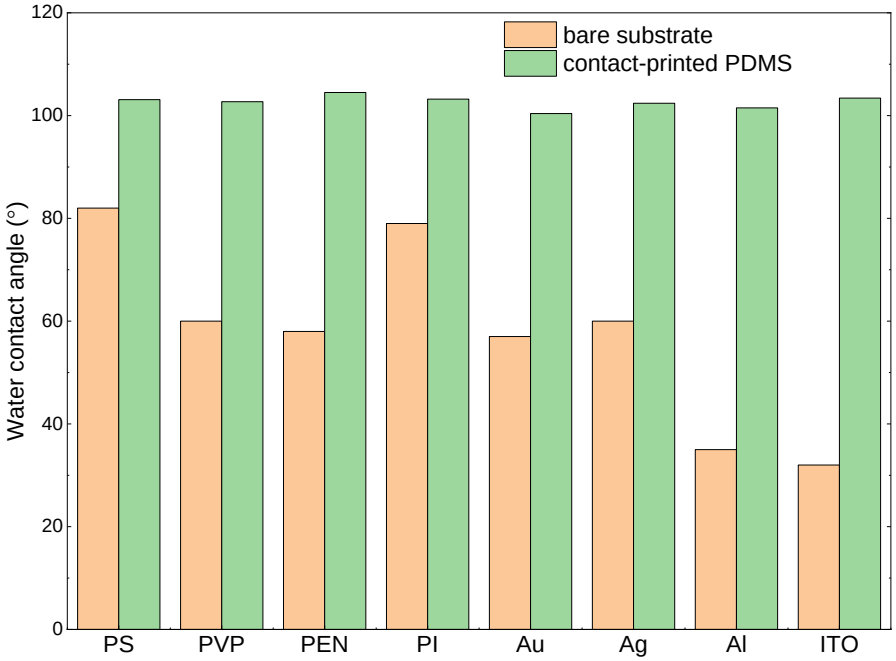

Figure S16. Water contact angle results for a contact-printed low-Mw PDMS layer on the various types of substrates. All of the PDMS layers show the same saturated contact angle of ~103°, which means the printed low-Mw PDMS layer could be derived by the same formation mechanism with same thickness irrespective of the type of material (see details in section Supplementary Information S4 above).

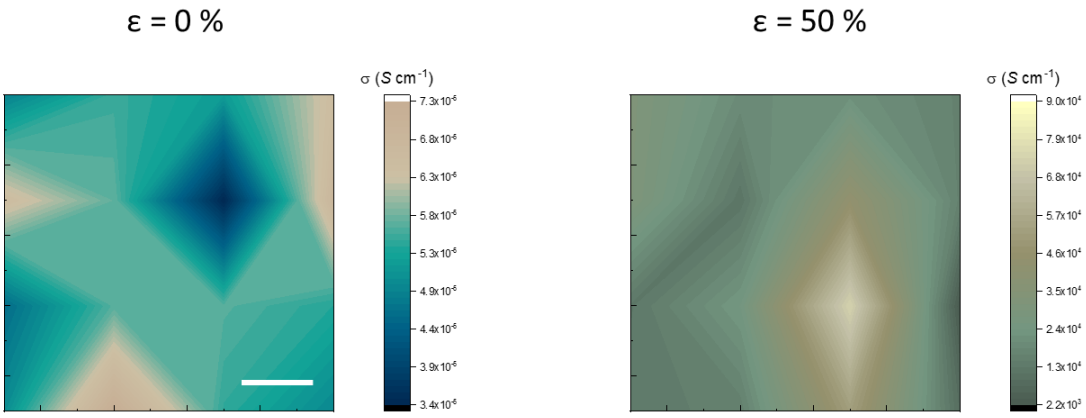

Figure S17. Mapping of conductivity on the mechanical strain gated electric switch. The switching ratio was uniform throughout the whole area (5 cm x 5 cm). Scale bar 1 cm.

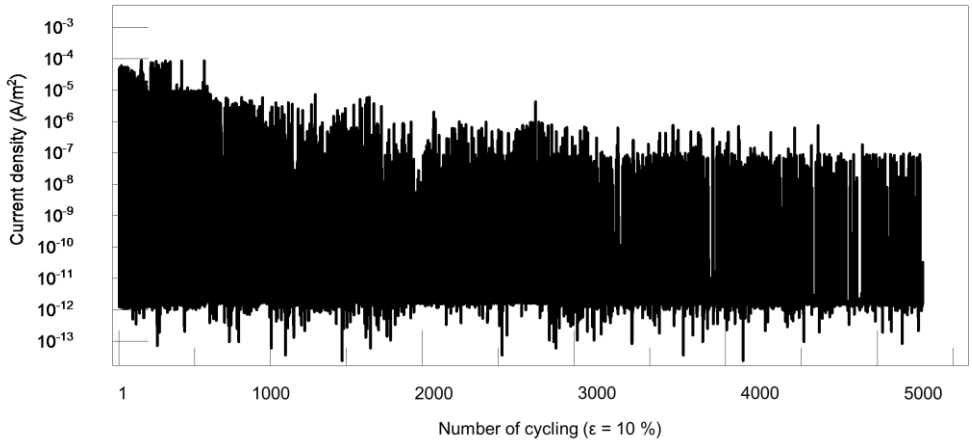

Figure S18. On-switching performance as a function of repeated stretching and releasing cycles up to 5,000 at a given applied strain (ε = 10 %). The operation of on-switching upon stretching remains unchanged after the initial training phase of about 1,500 stretching cycles.

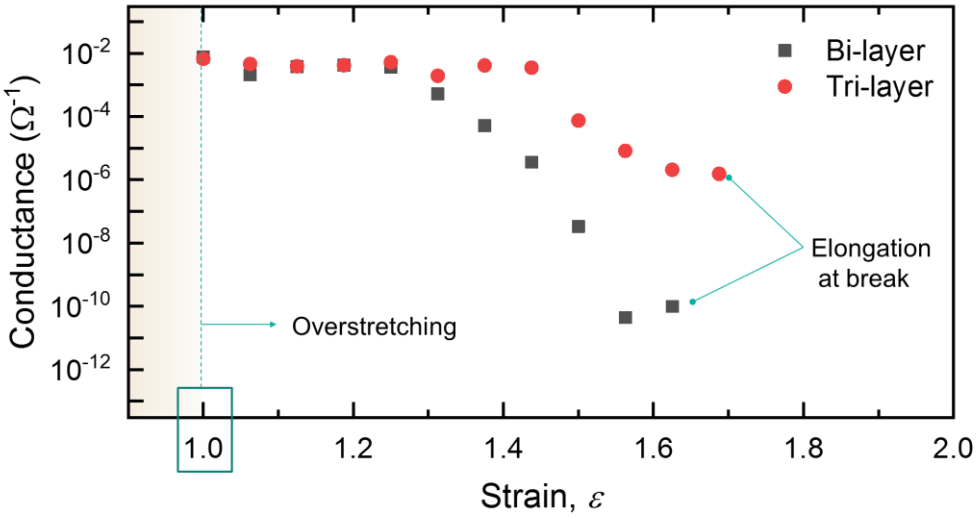

Figure S19. Conductivity decreasing of on-switch device at overstretching (ε > 1.3), which might be due to the reduction of the number of metal islands per unit area. Further studies employing more metal and intermediate layer (marked as Tri-layer) to increase the specific number of metal island per unit area, can be performed to increase the overstretching limitation.

Movie S1. “On” state of an LED bulb upon application of strain to a stretchable bilayer design showing the strain-gated electric on-switch behavior. The initial “off” state without strain and the switching behavior upon application of strain are shown.